

Experimental demonstration of topological error correction

Xing-Can Yao,¹ Tian-Xiong Wang,¹ Hao-Ze Chen,¹ Wei-Bo Gao,¹ Austin G. Fowler,² Robert Raussendorf,³ Zeng-Bing Chen,¹ Nai-Le Liu,¹ Chao-Yang Lu,¹ You-Jin Deng,¹ Yu-Ao Chen,¹ and Jian-Wei Pan¹

¹*Hefei National Laboratory for Physical Sciences at Microscale and Department of Modern Physics, University of Science and Technology of China, Hefei, Anhui 230026, PR China*

²*CQC2T, School of Physics, University of Melbourne, VIC 3010, Australia*

³*Department of Physics and Astronomy, University of British Columbia, Vancouver, BC, V6T 1Z1, Canada*

(Dated: November 27, 2024)

Scalable quantum computing can only be achieved if qubits are manipulated fault-tolerantly. Topological error correction—a novel method which combines topological quantum computing and quantum error correction—possesses the highest known tolerable error rate for a local architecture. This scheme makes use of cluster states with topological properties and requires only nearest-neighbour interactions. Here we report the first experimental demonstration of topological error correction with an eight-photon cluster state. It is shown that a correlation can be protected against a single error on any qubit, and when all qubits are simultaneously subjected to errors with equal probability, the effective error rate can be significantly reduced. This demonstrates the viability of topological error correction. Our work represents the first experimental effort to achieve fault-tolerant quantum information processing by exploring the topological properties of quantum states.

Quantum computers exploit the laws of quantum mechanics, and can solve many problems exponentially more efficiently than their classical counterparts [1–3]. However, in the laboratory, the ubiquitous decoherence makes it notoriously hard to achieve the required high degree of quantum control. To overcome this problem, quantum error correction (QEC) has been invented [4–6]. The capstone result in QEC, the so-called threshold theorem [7, 8], states that as long as the error rate p per gate in a quantum computer is smaller than a threshold value p_c , arbitrarily long and accurate quantum computation is efficiently possible. Unfortunately, most methods of fault-tolerant quantum computing with high threshold ($10^{-4} - 10^{-2}$) require strong and long-range interactions [7–9], and are thus difficult to implement. Local architectures are normally associated with much lower thresholds. For traditional concatenated codes on a 2D lattice of qubits with nearest-neighbour gates, the best threshold known to date [10] is 2.02×10^{-5} .

In such lattices, it is advantageous to employ topological error correction (TEC) [12–15, S2] in the framework of topological cluster-state quantum computing. This scheme makes use of the topological properties in three-dimensional (3D) cluster states, which form an inherently error-robust “fabric” for computation. Local measurements drive the computation and, at the same time, implement the error correction. Active error correction and topological methods are combined, yielding a high error threshold [12, 13] of 0.7%–1.1% and tolerating loss rates [15] up to 24.9%. This leaves room for the unavoidable imperfections of physical devices, and makes TEC close to the experimental state of the art. The 3D architecture can be further mapped onto a local setting in two spatial dimensions plus time [14], also with nearest-neighbour interactions only. Two detailed architectures have already been proposed [16, 17]. Note that a distinct and also important topological scheme has been proposed, in which

quantum computation is driven by non-abelian anyons [18, 19] and fault tolerance is achieved via passive stabilization afforded by a ground-state energy gap.

Some simple QEC codes have been experimentally demonstrated in nuclear magnetic resonance [20, 21], ion traps [22, 23] and optical systems [24, 25]. However, the experimental realization of topological QEC methods still remains a challenging task. The state-of-the-art technology for generating multipartite cluster state is up to six photons, while great endeavor is still underway to create non-abelian anyons for the topological quantum computing [18, 19]. Here, we develop an ultra-bright entangled-photon source by utilizing an interferometric Bell-type synthesizer. Together with a noise-reduction interferometer, we generate a polarization-encoded eight-photon cluster state, which is shown to possess the required topological properties for TEC. In accordance with the TEC scheme, we measure each photon (qubit) locally. Error syndromes are constructed from the measurement outcomes, and one topological quantum correlation is protected. We demonstrate: (1), if only one physical qubit suffers an error, the noisy qubit can be located and corrected, and (2), if all qubits are simultaneously subjected to errors with equal probability, the effective error rate is significantly reduced by error correction. Therefore, we have successfully carried out a proof-of-principle experiment that demonstrates the viability of *Topological Error Correction*—a central ingredient in topological cluster-state computing.

Cluster states and quantum computing

In cluster-state quantum computing [26], projective one-qubit measurements replace unitary evolution as the elementary process driving a quantum computation. The computation begins with a highly entangled multi-qubit

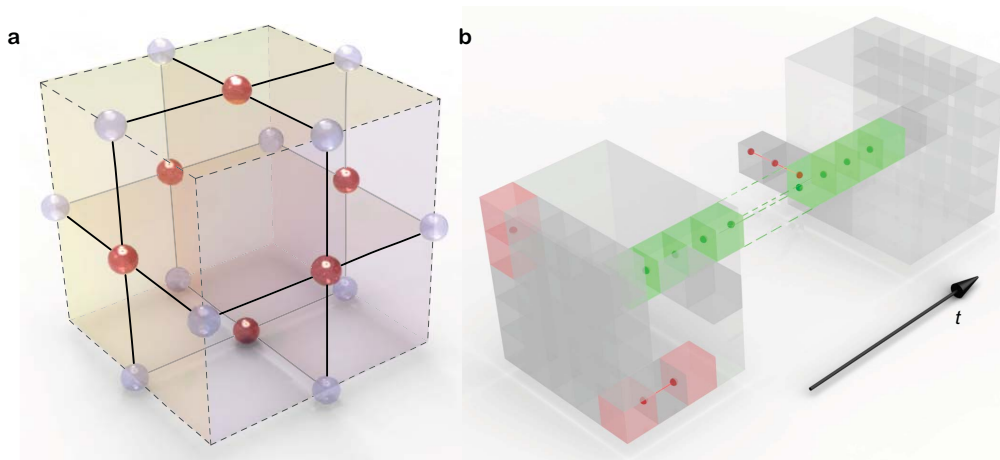


FIG. 1: **Topological cluster states.** The elementary lattice cell. Dashed lines represent the edges of the associated cell complex, while solid lines are for the edges of the interaction graph. Qubits live on the faces and the edges of the elementary cell. **b**, A larger topological cluster state of $5 \times 5 \times T$ cells. Green dots represent local Z measurements, effectively removing these qubits from the cluster state and thereby creating a non-trivial topology capable of supporting a single correlation. Red dots represent Z errors. Red cells indicate $C_F = -1$ at the ends of error chains. One axis of the cluster can be regarded as simulating the “circuit time” t . The evolution of logical states from t_1 to t_2 is achieved by performing local X measurements on all physical qubits between t_1 and t_2 .

state, the so-called cluster state $|G\rangle$ [27], which is specified by an interaction graph G and can be created from a product state via the pairwise Ising interaction over the edges in G . For each vertex $i \in G$, one defines a stabilizer as $K_i := X_i \otimes_{e_{ij}} Z_j$, where the product is over all the interaction edges e_{ij} connecting vertex i to its neighbouring vertex j . As usual, symbols X_i and Z_j denote the bit- and phase-flip Pauli operators, respectively, acting on qubits i and j . State $|G\rangle$ is the unique joint eigenstate of a complete set of stabilizers K_i , $K_i |G\rangle = |G\rangle$, for all the vertices $i \in G$.

Cluster states in $d \geq 3$ dimensions are resources for universal fault-tolerant quantum computing [12]. Therein, the TEC capability—shared with Kitaev’s toric code [28, S2] and the color code [29]—is combined with the capability to process quantum information.

Topological error correction

Quantum error correction and fault-tolerant quantum computing are possible with cluster states whenever the underlying interaction graph can be embedded in a 3D cell structure known as a cell complex [30], which consists of volumes, faces, edges and vertices. Qubits live on the edges and faces of a cell complex. The associated interaction graph connects the qubit on each face to the qubits on its surrounding edges via the interaction edges. Consider the elementary cell complex in Fig. 1a, shown by the dashed lines, it has 1 cubic volume, 6 square faces, 12 edges, and 8 vertices. The interaction edges, specified by the solid lines, form an 18-

qubit cluster state $|G_{18}\rangle$. There are 6 face stabilizers K_f ($f = 1, 2, \dots, 6$). It follows that multiplication of these stabilizers cancels out all Z operators in K_f and thus yields a unit expectation value $\langle X_1 X_2 \dots X_6 \rangle = 1$. This leads to a straightforward but important observation that despite the X -measurement on each individual face-qubit having random outcome ± 1 , the product of all the outcomes on any *closed* surface F is $+1$. Namely, any closed surface has the topological quantum correlation $C_F := \langle \otimes_{f \in F} X_f \rangle = 1$.

A larger cell complex is displayed in Fig. 1b, which encodes and propagates a logical qubit. It consists of $5 \times 5 \times T$ cells, with T specifying a span of simulated time t . A “defect” along the t direction (shown as the line of green dots in Fig. 1b) is first carved out via performing local Z measurements. Then, the topological quantum correlation $C_{F_D} = 1$ on a defect-enclosing closed surface, combined with the boundary, is used to encode a logical qubit. The evolution of the logical state from t_1 to t_2 is achieved by local X measurements on all other physical qubits between t_1 and t_2 (see Ref. [31] for the details). Quantum computing requires a much larger cell complex and more defects, where quantum algorithms are realized by appropriate braiding-like manipulation of defects (a sketch for the logical CNOT gate is shown in Appendix).

The quantum computation is possible precisely due to the topological quantum correlation $C_{F_D} = 1$ on defect-enclosing *closed* surfaces F_D . The TEC capability arises from the \mathbf{Z}_2 homology, a topological feature, of a sufficiently large 3D cell complex (see Appendix). For a given defect-enclosing closed surface F_D , there exist many homologically equivalent closed surfaces that represent the same topological correlation $C_{F_D} = 1$. This redundancy

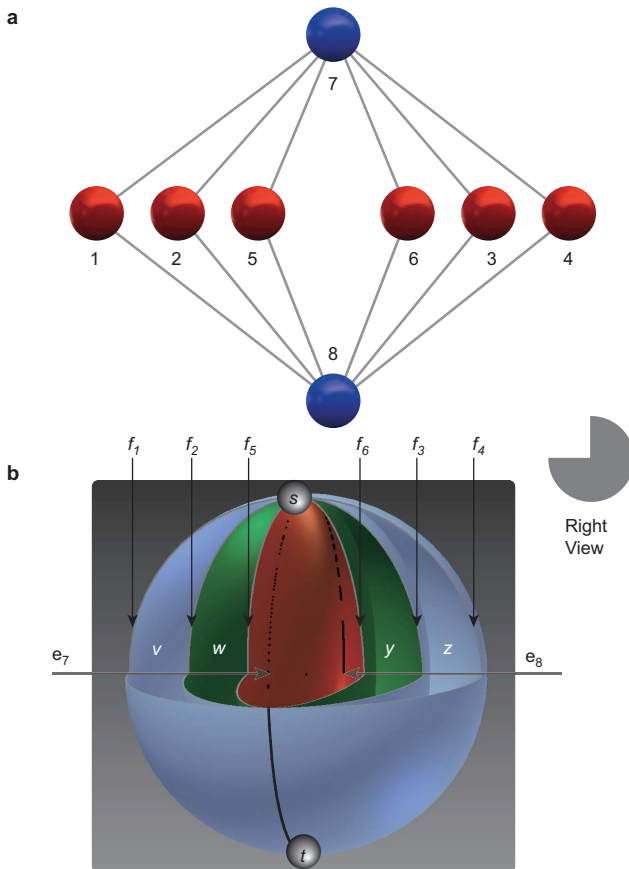


FIG. 2: **Cluster state $|G_8\rangle$ and its cell complex.** **a** Interaction graph G_8 of $|G_8\rangle$. **b**, The corresponding three-dimensional cell complex, with volumes v, w, y, z , faces $f_1, f_2, f_3, f_4, f_5, f_6$, edges e_7, e_8 , and vertices s, t . The exterior and the center volume are not in the complex. For better illustration, the cell complex is cut open and the front up quarter is removed, c.f. “right view”.

leads to the topological protection of the correlation [12].

Remarkably, in TEC it is sufficient to deal with Z errors, because an X error has either no effect if immediately before X measurements or is equivalent to multiple Z errors. Finally, as a measurement-based quantum computation, corrections suggested by TEC are not applied to the remaining cluster state but rather to the classical outcomes of X measurements.

Simpler topological cluster state

The cell complex in Fig. 1b encodes a propagating logical qubit via one topological correlation $C_{FD} = 1$, and is robust against a local Z error. Unfortunately, it contains 180 physical qubits per layer, significantly beyond the reach of available techniques. We design a simpler graph state $|G_8\rangle$, shown in Fig. 2a, to mimic the cell complex

TABLE I: Location of a Z error in $|G_8\rangle$ and the syndromes $C_{12} = \langle X_1 X_2 \rangle$ etc.

Z error	C_{12}	C_{25}	C_{36}	C_{34}
1	-1	1	1	1
2	-1	-1	1	1
3	1	1	-1	-1
4	1	1	1	-1
5	1	-1	1	1
6	1	1	-1	1

of Fig. 1b.

The topological feature of $|G_8\rangle$ can be seen via its association with the 3D cell complex in Fig. 2b, which consists of 4 elementary volumes $\{v, w, y, z\}$, 6 faces $\{f_1, f_2, f_3, f_4, f_5, f_6\}$, 2 edges $\{e_7, e_8\}$, and 2 vertices $\{s, t\}$. All 6 faces have the same boundary $e_7 \cup e_8$, and any two of them forms a closed surface F . The center volume is carved out, resembling the defect in Fig. 1b, and the to-be-protected topological correlation C_{FD} reads

$$C_{FD} := \langle X_5 X_6 \rangle = 1. \quad (1)$$

In this simple cell complex, the topological correlation $C_{FD} = 1$ is already multiply encoded, represented by any expectation $\langle X_i X_j \rangle$ with $i \in \{1, 2, 5\}$ and $j \in \{3, 4, 6\}$. Moreover, there exist four other closed surfaces without enclosing the defect, corresponding to the boundary of volumes v, w, y, z , respectively. The “redundant” topological correlations are

$$\langle X_1 X_2 \rangle = \langle X_2 X_5 \rangle = \langle X_3 X_6 \rangle = \langle X_3 X_4 \rangle = 1, \quad (2)$$

and can be used as error syndromes in TEC. As shown in Table 1, a single Z error on any physical qubit can be located and corrected.

Therefore, from the aspect of TEC capability, the cluster state $|G_8\rangle$ is analogous to the cell complex in Fig. 1b. They protect one topological correlation and are robust against a single Z error, albeit the cell complex in Fig. 2b is too small to propagate a logical qubit (see Appendix for detailed discussion).

Preparation of the eight-photon cluster state

In our experiment, the desired eight-qubit cluster state is created using spontaneous parametric down-conversion and linear optics. The first step is to develop an ultra-bright and high-fidelity entangled-photon source. As shown in Fig. 3a, an ultraviolet mode-locked laser pulse (915 mW) passes through a β -barium borate (BBO) crystal, generating a pair of polarization-entangled photons in the state $|\phi\rangle = (|HH\rangle + |VV\rangle)/\sqrt{2}$. By an interferometric Bell-state synthesizer [32], photons of different bandwidths (shown by red and blue dots in Fig. 3a, respectively) are guided through separate paths. This

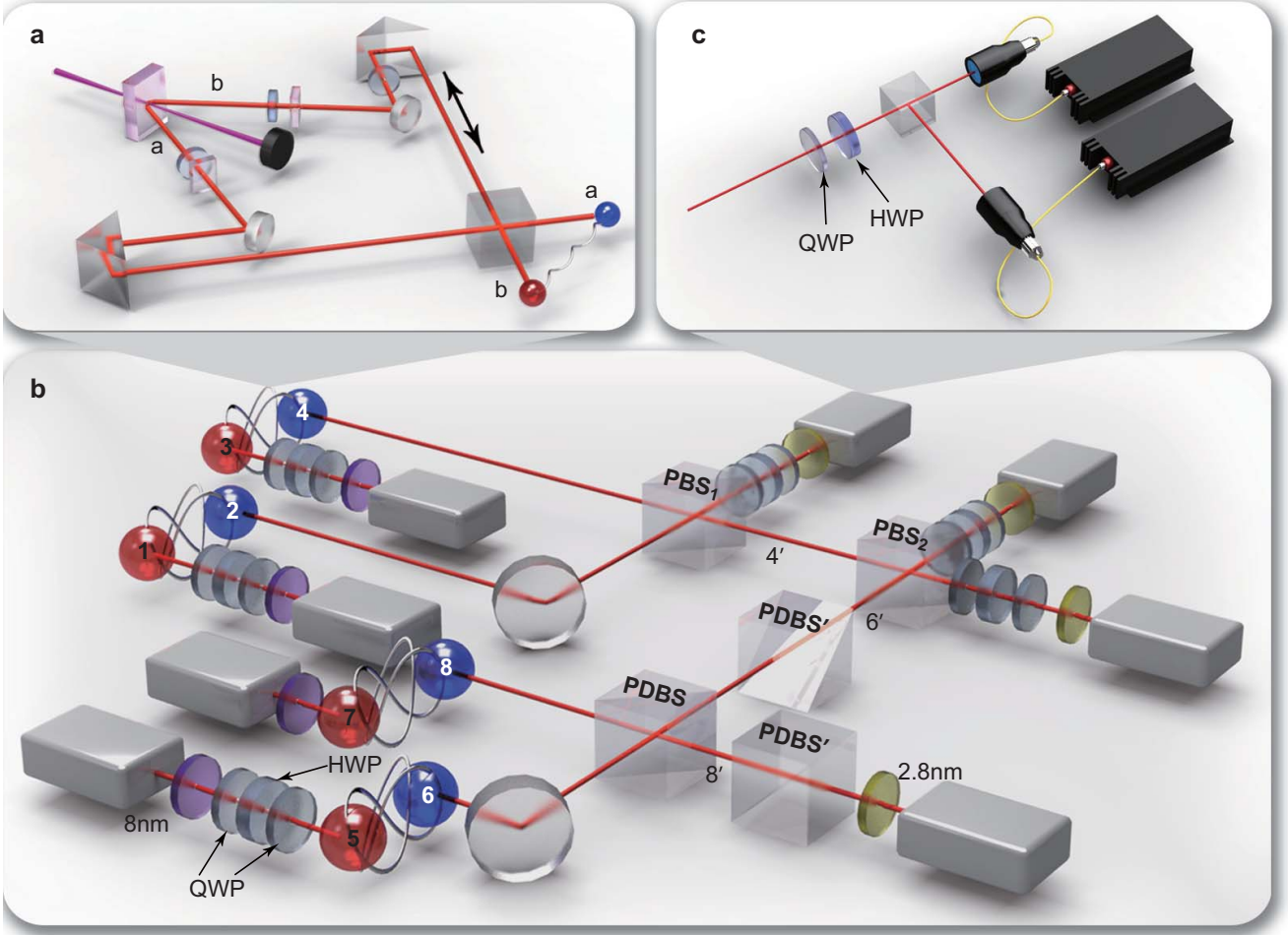


FIG. 3: **Experimental setup for the generation of the eight-photon cluster state and the demonstration of topological error correction.** **a** Creation of ultra-bright entangled photon pairs. An ultraviolet laser pulse passes through a 2 mm nonlinear BBO crystal, creating an entangled photon pair by parametric down conversion with $\rho = \frac{1}{2}(|H_a^o\rangle|V_b^e\rangle\langle V_b^e| + \langle H_a^o| + |V_a^e\rangle\langle H_b^o| + \langle V_a^e|)$, where o and e indicate the polarization with respect to the V -polarized pump. After both photons pass through compensators including a 45° HWP and a 1 mm BBO crystal, one of the photons' polarizations is rotated by another 45° HWP. Then we re-overlap the two photons on a PBS, creating an entangled photon pair with $|\phi_{ab}\rangle = \frac{1}{\sqrt{2}}(|H\rangle|H\rangle + e^{i\varphi}|V\rangle|V\rangle) \otimes |e_a\rangle|o_b\rangle$. **b**, In order to create the desired cluster state, we combine photons from path 6 and 8 at PDBS and let each photon pass through another PDBS', resulting a controlled-phase operation between photon 6 and 8. Meanwhile photon 2 and photon 4 are interfered on PBS₁. In the end, photon 4' and photon 6' are overlapped on PBS₂. Upon a coincidence detection, we create the eight-photon cluster state (3) for topological error correction. **c**, Polarization analyzer for each individual photon, containing a QWP, an HWP, a PBS and two single-mode fibre-coupled single-photon detectors.

disentangles the temporal from the polarization information. In contrast to the conventional narrow-band filtering technique, there is no photon-loss problem, and thus an ultra-high brightness is achieved. Four pairs of such entangled photons are prepared and labelled as 1-2, 3-4, 5-6 and 7-8 in Fig. 3b. Then, we generate two graph states, each of four photons. The first one is a four-photon GHZ state $(|H^{\otimes 4}\rangle_{1-4} + |V^{\otimes 4}\rangle_{1-4})/\sqrt{2}$, obtained by superposing photon 2 and photon 4 on a polarizing beam-splitter (PBS₁) which transmits H and reflects V polarization. Meanwhile, photon 6 and photon 8 are interfered on a polarization-dependent beam-splitter

(PDBS) and then separately pass through two PDBS. The former has transmitting probabilities $T_H = 1$, $T_V = 1/3$ and the latter have $T_H = 1/3$, $T_V = 1$. The combination of these three PDBSs acts as a controlled-phase gate [33, 34]. With a success probability of $1/9$, one has the twofold coincidence in path 6' and 8', yielding a four-photon cluster state [34] $[|HH\rangle_{56}(|HH\rangle_{78} + |VV\rangle_{78}) + |VV\rangle_{56}(|HH\rangle_{78} - |VV\rangle_{78})]/2$. Finally, photon 4' and photon 6' are superposed on PBS₂. When eight photons come out of the output ports simultaneously, one obtains an entangled eight-photon cluster state:

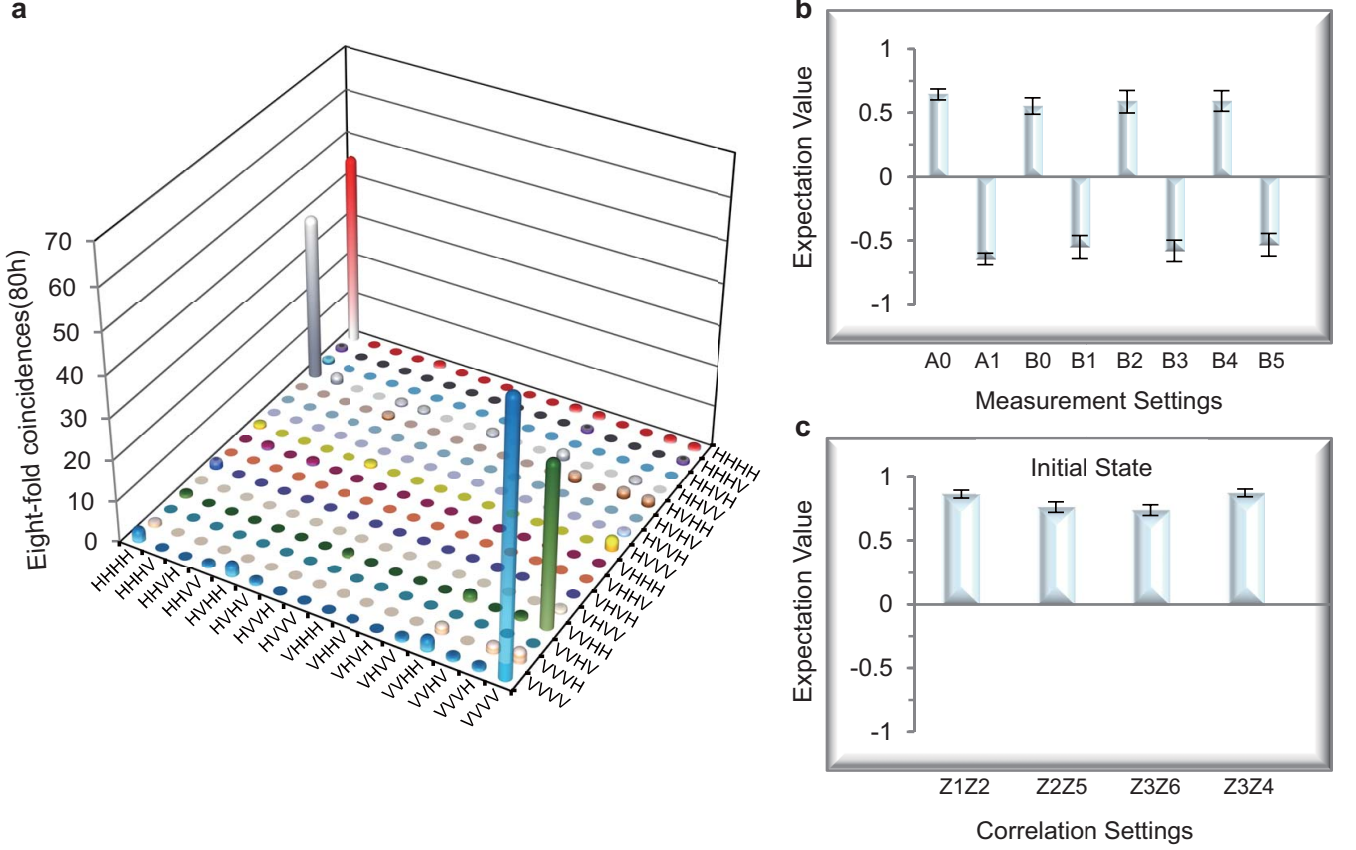


FIG. 4: **Experimental results for the created eight-photon cluster state.** **a**, Measured eight-fold coincidence in $|H\rangle/|V\rangle$ basis. **b**, The expectation values for different witness measurement settings. From left to right, the measurement settings are $A_0 = (|H\rangle\langle H|^{\otimes 6} - |V\rangle\langle V|^{\otimes 6})_{1-6} X_7 X_8$, $A_1 = (|H\rangle\langle H|^{\otimes 6} - |V\rangle\langle V|^{\otimes 6})_{1-6} Y_7 Y_8$, and $B_i = M_i^{\otimes 6} (|H\rangle\langle H|^{\otimes 2} - |V\rangle\langle V|^{\otimes 2})_{78}$ with $i = 0, \dots, 5$. The measurement of each setting takes 50 hours for the first two settings and 30 hours for the remainings. **c**, Correlations for initial state without any engineered error. The error bars represent one standard deviation, deduced from propagated poissonian counting statistics of the raw detection events.

$$|\psi\rangle = \frac{1}{2} [|H^{\otimes 6}\rangle_{1-6} (|HH\rangle_{78} + |VV\rangle_{78}) + |V^{\otimes 6}\rangle_{1-6} (|HH\rangle_{78} - |VV\rangle_{78})]. \quad (3)$$

This is exactly the cluster state $|G_8\rangle$ shown in Fig. 2a under Hadamard operations $H^{\otimes 8}$ on all qubits. Note that the photons, which are interfered on the PBSs or at the PDBS, have the same bandwidth, and a star topology of the eight-photon interferometer leads to an effective noise-reduction.

To ensure good spatial and temporal overlap, the photons are also spectrally filtered, with $\Delta\lambda_{\text{FWHM}} = 8$ nm for 1-3-5-7 and $\Delta\lambda_{\text{FWHM}} = 2.8$ nm for 2-4-6-8, and coupled by single-mode fibres. We obtain an average two-fold coincidence count of about 3.4×10^5 /s and a visibility of $\sim 94\%$ in the $|H\rangle/|V\rangle$ as well as in the $|+\rangle/|-\rangle$ basis, where $|\pm\rangle = \frac{1}{\sqrt{2}} (|H\rangle \pm |V\rangle)$. Fine adjustments of the delays between the different paths are tuned to en-

sure that all the photons arrive at the PBSs and PDBS simultaneously.

Measurement is taken for each individual photon by a polarization analyzer, which contains a combination of a QWP, a HWP and a PBS, together with two single-mode fibre-coupled single-photon detectors in each output of the PBS (see Fig. 3c). The complete set of the 256 possible combinations of eight-photon coincidence events is registered by a home-made FPGA-based programmable coincidence logic unit. We obtain an eight-fold coincidence rate of 3.2 per hour. Based on the measurements for the 256 possible polarization combinations in the $|H\rangle/|V\rangle$ basis (Fig. 4a), we obtain a signal-to-noise ratio of about 200:1, defined as the ratio of the average of

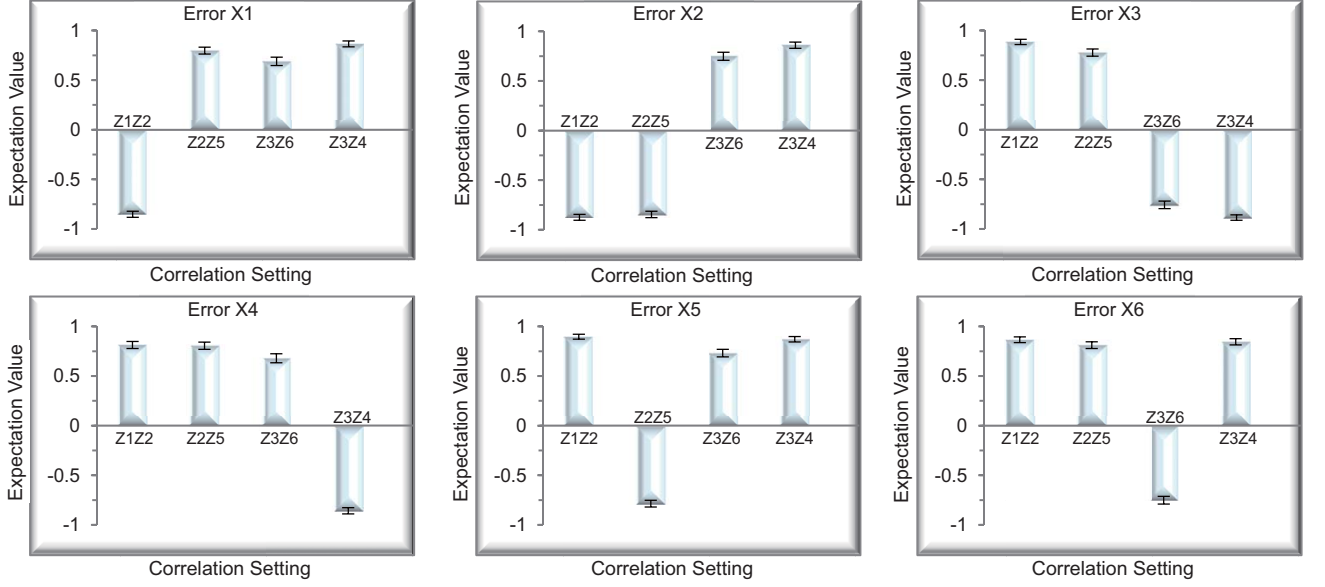


FIG. 5: **Experimental results of syndrome correlations for topological error correction.** Only one qubit is subjected to an X error in each sub-figure. The measurement for each error setting takes about 80 hours. The error bars represent one standard deviation, deduced from propagated poissonian counting statistics of the raw detection events.

the desired components to that of the non-desired ones. This indicates the success of preparing the desired eight-photon cluster state.

To more precisely characterize the cluster state, we use the entanglement-witness method to determine its fi-

delity. For this purpose, we construct a witness which allows for the lower bound on the state fidelity and requires only eight measurement settings (see Appendix):

$$\begin{aligned}
 \mathcal{W}_8 &= \frac{1}{2} - (|\psi\rangle\langle\psi| - |\psi'\rangle\langle\psi'|) \\
 &= \frac{1}{2} - \left[\frac{1}{4} (|H\rangle\langle H|^{\otimes 6} - |V\rangle\langle V|^{\otimes 6})_{1-6} \otimes (X_7 X_8 - Y_7 Y_8) + \right. \\
 &\quad \left. \frac{1}{12} \left(\sum_{k=0}^5 (-1)^k M_k^{\otimes 6} \right)_{1-6} \otimes (|H\rangle\langle H|^{\otimes 2} - |V\rangle\langle V|^{\otimes 2})_{78} \right], \tag{4}
 \end{aligned}$$

where $\langle\psi'|\psi\rangle = 0$ and $M_k = [\cos(\frac{k\pi}{6})X + \sin(\frac{k\pi}{6})Y]$. The results are shown in Fig. 4b, which yields the witness $\langle W \rangle = -0.105 \pm 0.023$, which is negative by 4.5 standard deviations. The state fidelity is $F > \frac{1}{2} - \langle W \rangle = 0.605 \pm 0.023$. The presence of genuine eight-photon entanglement is confirmed.

Experimental topological error correction

Given such a cluster state, topological error correction is implemented using a series of single-qubit measure-

ments and classical correction operations. In the laboratory, operations are performed on state (3), differing from $|G_8\rangle$ in Fig. 2a by Hadamard operation $H^{\otimes 8}$. Therefore, the to-be-protected correlation $\langle X_5 X_6 \rangle$ in Eq. (1) corresponds to $\langle Z_5 Z_6 \rangle$ in the experiment; the same applies to the syndrome correlations (2). Meanwhile, X errors are engineered instead of Z errors.

In the experiment, the noisy quantum channels on polarization qubits are engineered by one HWP sandwiched with two QWPs, which are set at 90 degrees. By randomly setting the HWP axis to be oriented at $\pm\theta$ with respect to the horizontal direction, the noisy quantum

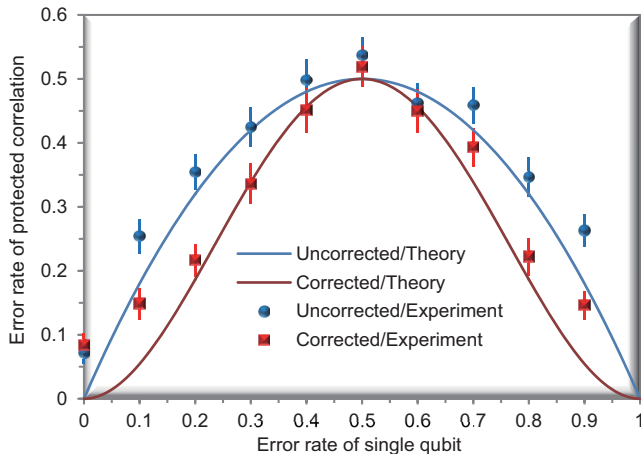


FIG. 6: **Experimental results of topological error correction.** All physical qubits are simultaneously subject to an X error with equal probability ranging from 0 to 1. The blue round dots (blue lines) represent the experimental (theoretical) values of the error rate for the protected correlation without TEC, and the red square dots (red lines) are for the error rate with TEC. The agreement between the experimental and the theoretical results clearly demonstrates the viability of TEC. The measurement of each data point takes 80 hours. The error bars represent one standard deviation, deduced from propagated poissonian counting statistics of the raw detection events.

channel can be engineered with a bit-flip error probability of $p = \sin^2(2\theta)$.

We first study the case that only a single X error occurs on one of the six photons $\{1, \dots, 6\}$. The syndrome correlations are measured, and the results are shown in Fig. 5. For comparison, we also plot the correlations without any engineered error in Fig. 4c. Indeed, one can precisely locate the physical qubit undergoing an X error.

We then consider the case that all the six photons are simultaneously subject to a random X error with equal probability $0 < p < 1$, and study the rate of errors, $\langle Z_5 Z_6 \rangle = -1$, for the topological quantum correlation $\langle Z_5 Z_6 \rangle$. Without error correction, the error rate of correlation $\langle Z_5 Z_6 \rangle$ is $P = 1 - (1 - p)^2 - p^2$. With error correction, the residual error becomes

$$P = 1 - [(1 - p)^6 + p^6] - [6p(1 - p)^5 + 6(1 - p)p^5] - [9p^2(1 - p)^4 + 9(1 - p)^2p^4]. \quad (5)$$

For small p , the residual error rate after error correction is significantly reduced as compared to the unprotected case. As shown in Fig. 6, the experimental results are in good agreement with these theoretical predictions. Considerable improvement of the robustness of the $\langle Z_5 Z_6 \rangle$ correlation can be seen both in theory and in practice.

In the experiment, the whole measurement takes about 80 days. This requires an ultra stability of our setup. The imperfections in the experiment are mainly due to the undesired components in the $|H\rangle/|V\rangle$ basis, arising from higher-order emissions of entangled photons, and the imperfect photon overlapping at the PBSs and the PDBS. In spite of these imperfections, the viability of TEC is clearly demonstrated in the experiment.

Discussion

In the current work, we have experimentally demonstrated TEC with an eight-photon cluster state. This state represents the current state-of-the-art for preparation of cluster states in any qubit system and is of

particular interest in studying multipartite entanglement and quantum information processing. The scalable construction of cluster states in the future will require further development of high-efficiency entanglement sources and single-photon detectors [35]. Recent results have shown that if the product of the number-resolving detector efficiency and the source efficiency is greater than $2/3$, efficient linear optical quantum computation is possible [36]. Solid technical progress towards this goal has been made such as deterministic storable single-photon sources [37] and photon-number-resolving detectors [38]. This work represents the first experimental demonstration of TEC, an important step towards fault-tolerant quantum computation. In the scheme, given sufficient qubits and physical error rates below 0.7%–1.1%, arbitrary quantum computations could be performed arbitrarily reliably. The high threshold error rate is especially remarkable given that only nearest neighbour interactions are required. Due to these advantages, TEC is especially well-suited for physical systems geometrically constrained to nearest-neighbour interactions, such as quantum dots [39], Josephson junction qubits [40], ion

traps [41], cold atoms in optical lattices [42] and photonic modules [17]. A quantum gate with an error rate below the threshold required in TEC is within reach of current experimental technology [43]. It would be interesting in future work to exploit cluster states of reachable size to implement topologically error-protected quantum algorithms by local measurements.

We acknowledge insightful discussions with M. A.

Martin-Delgado, O. Gühne. We are grateful to X.-H. Bao for his original idea of the ultra-bright entanglement and to C.-Z. Peng for his idea of reducing high order emission. We would also like to thank C. Liu and S. Fölling for their help in designing the figures. This work has been supported by the NNSF of China, the CAS, the National Fundamental Research Program (under Grant No. 2011CB921300) and NSERC.

-
- [1] Shor, P. W. Polynomial-time algorithms for prime factorization and discrete logarithms on a quantum computer. In *Proceedings of the 35th Annual Symposium on Foundations of Computer Science* (1994).
- [2] Grover, L. K. Quantum mechanics helps in searching for a needle in a haystack. *Phys. Rev. Lett.* **79**, 325 (1997).
- [3] Feynman, R. P. Simulating physics with computers. *Int. J. Theor. Phys.* **21**, 467–488 (1982).
- [4] Calderbank, A. R. & Shor, P. W. Good quantum error-correcting codes exist. *Phys. Rev. A* **54**, 1098–1105 (1996).
- [5] Steane, A. M. Error correcting codes in quantum theory. *Phys. Rev. Lett.* **77**, 793–797 (1996).
- [6] Gottesman, D. Theory of fault-tolerant quantum computation. *Phys. Rev. A* **57**, 127–137 (1998).
- [7] Knill, E. Quantum computing with realistically noisy devices. *Nature* **434**, 39–44 (2005).
- [8] Aliferis, P., Gottesman, D. & Preskill, J. Quantum accuracy threshold for concatenated distance-3 code. *Quant. Inf. Comput.* **6**, 97–165 (2006).
- [9] Kitaev, A. Y. Quantum computations: Algorithms and error correction. *Russ. Math. Surv.* **52**, 1191–1249 (1997).
- [10] Spedalieri, F. & Roychowdhury, V. P. Latency in local, two-dimensional, fault-tolerant quantum computing. *Quant. Inf. Comput.* **9**, 666–682 (2009).
- [11] Dennis, E., Landahl, A., Kitaev, A. & Preskill, J. Topological quantum memory. *J. Math. Phys.* **43**, 4452–4505 (2002).
- [12] Raussendorf, R., Harrington, J. & Goyal, K. A fault-tolerant one-way quantum computer. *Ann. Phys.* **321**, 2242–2270 (2006).
- [13] Wang, D. S., Austin, A. G. & Hollenberg, L. C. L. Quantum computing with nearest neighbor interactions and error rates over 1%. *Phys. Rev. A* **83**, R020302 (2011).
- [14] Raussendorf, R. & Harrington, J. Fault-tolerant quantum computation with high threshold in two dimensions. *Phys. Rev. Lett.* **98**, 190504 (2007).
- [15] Barrett, S. D. & Stace, T. M. Fault tolerant quantum computation with very high threshold for loss errors. *Phys. Rev. Lett.* **105**, 200502 (2010).
- [16] Stock, R. & James, D. F. V. A scalable, high-speed measurement-based quantum computer using trapped ions. *Phys. Rev. Lett.* **102**, 170501 (2009).
- [17] Devitt, S. J. *et al.* Topological cluster state computation with photons. *New J. Phys.* **11**, 083032 (2009).
- [18] Nayak, C., Simon, S. H., Stern, A., Freedman, M. & Sarma, S. D. Non-abelian anyons and topological quantum computation. *Rev. Mod. Phys.* **80**, 1083–1159 (2008).
- [19] Wilczek, F. *Fractional Statistics and Anyon Superconductivity* (World Scientific, Singapore, 1990).
- [20] Cory, D. G. *et al.* Experimental quantum error correction. *Phys. Rev. Lett.* **81**, 2152–2155 (1998).
- [21] Knill, E., Laflamme, R., Martinez, R. & Negrevergne, C. Benchmarking quantum computers: The five-qubit error correcting code. *Phys. Rev. Lett.* **86**, 5811–5814 (2001).
- [22] Chiaverini, J. *et al.* Realization of quantum error correction. *Nature* **432**, 602–605 (2004).
- [23] Schindler, P. *et al.* Experimental repetitive quantum error correction. *Science* **332**, 1059–1061 (2011).
- [24] Lu, C.-Y. *et al.* Experimental quantum coding against qubit loss error. *Proc. Natl. Acad. Sci. USA* **105**, 11050–11054 (2008).
- [25] Aoki, T. *et al.* Quantum error correction beyond qubits. *Nature Physics* **5**, 541–546 (2009).
- [26] Raussendorf, R. & Briegel, H. J. A one-way quantum computer. *Phys. Rev. Lett.* **86**, 5188–5191 (2001).
- [27] Schlingemann, D. & Werner, R. F. Quantum error-correcting codes associated with graphs. *Phys. Rev. A* **65**, 012308 (2001).
- [28] Kitaev, A. Y. Fault-tolerant quantum computation by anyons. *Ann. Phys.* **303**, 2–30 (2003).
- [29] Bombin, H. & Martin-Delgado, M. A. Topological quantum distillation. *Phys. Rev. Lett.* **97**, 180501 (2006).
- [30] Hatcher, A. *Algebraic Topology*. (Cambridge University Press, Cambridge, UK, 2002).
- [31] Fowler, A. G. & Goyal, K. Topological cluster state quantum computing. *Quant. Inf. Comput.* **9**, 727–738 (2009).
- [32] Yao, X.-C. *et al.* Observation of eight-photon entanglement. *arXiv: 1105.6318v1 [quant-ph]* (2011).
- [33] Hofmann, H. F. & Takeuchi, S. Quantum phase gate for photonic qubits using only beam splitters and postselection. *Phys. Rev. A* **66**, 024308 (2002).
- [34] Kiesel, N. *et al.* Experimental analysis of a four-qubit photon cluster state. *Phys. Rev. Lett.* **95**, 210502 (2005).
- [35] O’Brien, J. L. Optical quantum computing. *Science* **318**, 1567–1570 (2007).
- [36] Varnava, M., Browne, D. E. & Rudolph, T. How good must single photon sources and detectors be for efficient linear optical quantum computation? *Phys. Rev. Lett.* **100**, 060502 (2008).
- [37] Chen, S. *et al.* Deterministic and storable single-photon source based on quantum memory. *Phys. Rev. Lett.* **97**, 173004 (2006).
- [38] Kardynal, B. E., Yuan, Z. L. & Shields, A. J. An avalanche-photodiode-based photon-number-resolving detector. *Nature Physics* **2**, 425–428 (2008).
- [39] Press, D. *et al.* Complete quantum control of a single quantum dot spin using ultrafast optical pulses. *Nature* **456**, 218–221 (2008).
- [40] Hime, T. *et al.* Solid-state qubits with current-controlled coupling. *Science* **314**, 1427–1429 (2006).
- [41] Hensinger, W. K. *et al.* T-junction ion trap array for two-dimensional ion shuttling, storage, and manipulation.

Appl. Phys. Lett. **88**, 034101 (2006).

[42] Jaksch, D. *et al.* Entanglement of atoms via cold controlled collisions. *Phys. Rev. Lett.* **82**, 1975–1978 (1999).

[43] Benhelm, J., Kirchmair, G., Roos, C. F. & Blatt, R. Towards fault-tolerant quantum computing with trapped ions. *Nature physics* **4**, 463–466 (2008).

Appendix

S.I. TOPOLOGICAL CLUSTER STATE QUANTUM COMPUTATION

a. Cluster states and homology. The topological feature of error-correction with three-dimensional (3D) cluster states is homology, which we shall illustrate in 2D for simplicity. Displayed in Fig. S1 is a 2D plane with two point defects (\bullet). The boundary of a surface is defined as the *sum* of all the surrounding chains. For instance, the boundary of the surface f (shown in blue) is the sum of e_1 and e_2 , denoted as $\partial f = e_1 + e_2$. Because of the presence of the point defects, each of the three chains, e_1 , e_2 , and e_3 , is not sufficient to be the whole boundary of a surface. Analogously, the boundary of a chain is defined as the sum of its endpoints. Since the three chains are cycles, they have no boundary—i.e., $\partial e_1 = \partial e_2 = \partial e_3 = 0$. The chain e_2 can be smoothly transformed into e_1 , and vice versa. In other words, e_1 and e_2 differ only by the boundary of a surface: $e_2 = e_1 + \partial f$. We say that e_1 and e_2 are homologically equivalent. In contrast, e_3 is inequivalent to e_1 or e_2 due to the defect on the right-hand side. The homology in higher dimensions is defined in an analogous way. In 3D, the boundary of a volume is the sum of all its surrounding surfaces. A closed surface F is said to have no boundary, i.e., $\partial F = 0$. A simple example is the surface of a sphere. Two surfaces F and F' are homologically equivalent if they differ only by the boundary of a volume V : $F' = F \pm \partial V$.

In topological cluster state computation, the error correction scheme only involves local measurements in the X basis, with outcomes $\lambda = \pm 1$. Computational results are represented by correlations $R(F) = \prod_{a \in F} \lambda_a$ of these outcomes on a closed surface F — $\partial F = 0$. As in any encoding, error-resilience is brought about by redundancy. A given bit of the computational result is inferred not only from a particular surface F , but from any one in a huge homology equivalence class. This arises because two homologically equivalent surfaces F and F' have the same correlation $R(F) = R(F')$ in the absence of errors [S1]. As a result, one has $R(\partial V) = 1$ for every volume V . An outcome of -1 then indicates the occurrence of an error in the volume V , and thus $R(\partial V)$ can be used as error syndromes. We obtain one bit of such error syndrome per lattice cell; c.f. Fig. 1a.

The errors have a geometrical interpretation, too. They correspond to 1-chains e [S2]. Again, homology becomes relevant: Two homologically equivalent error chains e and e' have the same effect on computation.

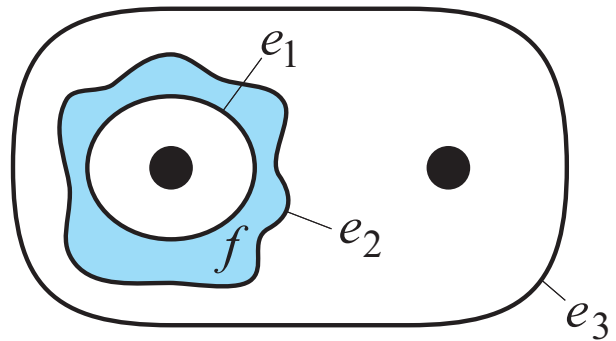


FIG. S1: **Illustration of homological equivalence in two dimensions.** Here is a 2D plane with two point defects (\bullet). All three chains, e_1 , e_2 , and e_3 , are cycles and thus have no boundary. They are furthermore nontrivial: each of them is insufficient to be the whole boundary of a surface. The cycles e_1 and e_2 are said to be homologically equivalent because they differ only by the boundary ∂f of the surface f . In contrast, e_3 is not equivalent to e_1 or e_2 . In other words, e_1 and e_2 can collapse into each other by *smooth* deformation, while e_3 cannot be smoothly transformed into e_2 or e_1 because of the presence of the right-hand-side defect. In the topological cluster state quantum computation, errors are represented by chains. two homologically equivalent error chains have the same effect on computation.

In topological error correction with cluster states, the computational results and the syndromes are contained in correlations among outcomes of local X -measurements. Detecting and correcting only phase flips of physical qubits is thus sufficient to correct arbitrary errors. Nevertheless, both bit flip and phase flip errors are present at the level of logical operations. The qubits in a 3D cluster state live on the faces and edges of the associated lattice. Logical phase errors are caused by erroneous measurement of face qubits, and logical spin flip errors are by erroneous measurement of edge qubits. For example, the 8-qubit cluster state $|G_8\rangle$ considered in this experiment has the correlation $\langle G_8 | X_2 \otimes X_2 | G_8 \rangle = 1$, in addition to the four correlations used as error syndromes for face qubits. It can be derived from a dual complex [S1], and provides one bit of (dual) syndrome for the edge qubits of \mathcal{L}_8 .

b. Topologically protected quantum gates. Topologically protected quantum gates are performed by measuring certain regions of qubits in the Z basis, which effectively removes them. The remaining cluster, whose qubits are to be measured in the X and $X \pm Y$ basis, thereby attains a non-trivial topology in which fault-tolerant quantum gates can be encoded. Fig. S2 shows a macroscopic view of a 3D sub-cluster for the realization of a topologically protected CNOT gate [S3, S4]. Only the topology of the cluster matters, individual lattice cells are not resolved. The cluster qubits in the line-like regions D are measured in the Z -basis, the remaining cluster qubits in the X -basis.

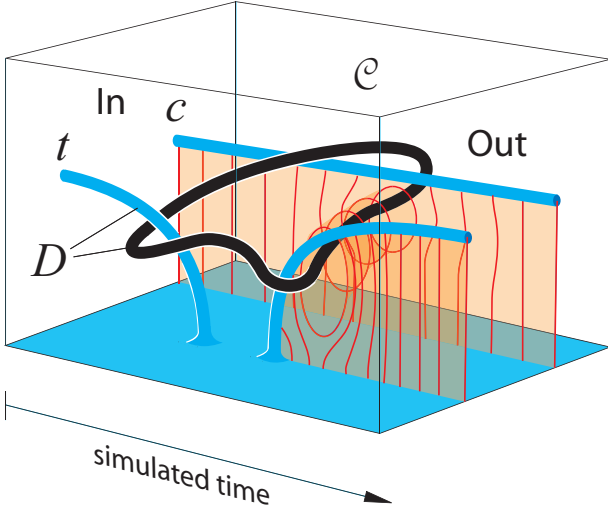


FIG. S2: **Topological gates with 3D cluster states.** The sub-cluster \mathcal{C} (indicated by the wire frame) realizes an encoded CNOT gate between control c and target t . The regions D are missing from the cluster. Each line-like such region supports the world-line of one encoded qubit. One of the four homologically non-trivial correlation surfaces for the encoded CNOT is shown in orange.

The fault-tolerance of measurement-based quantum computation with a 3D cluster state can be understood by mapping it to a Kitaev surface code propagating in time [S3]. In this picture, a 3D cluster state consists of many linked toric code surfaces plus extra qubits for code stabilizer measurement, entangled with these surfaces. The local measurements in each slice have the effect of teleporting the encoded state to the subsequent code surface. The code surfaces can support many encoded qubits because they have boundary. Encoded gates are implemented by changing the boundary conditions with time. This process is illustrated in Fig. S2 for the CNOT gate. Pieces of boundary in the code surface are created by the intersection of the line-like regions D with surfaces of “constant time”. The 1-chains displayed in

red represent encoded Pauli operators \bar{X} at a given instant of simulated time. When propagating forward, an initial operator \bar{X}_c is converted into $\bar{X}_c \otimes \bar{X}_t$ as required by conjugation under CNOT.

c. Further Reading. For the interested reader we add a few references. The topological error-correction capability in 3D cluster states is, for the purpose of establishing long-range entanglement in the presence of noise, discussed in [S5]. How to perform universal fault-tolerant quantum computation with 3D cluster states is described in [S1] and in terms of stabilizers in [S6]. In [S3], a mapping from three spatial dimensions to two spatial dimensions plus time is provided, and the fault-tolerance threshold is improved to 0.7%, for both the three and the two-dimensional version. The 2D scheme is described solely in terms of the toric code in [S7].

S.II. CHARACTERIZATION OF THE 8-QUBIT CLUSTER STATE

In order to characterize the generated 8-qubit cluster state, we use entanglement witnesses to verify its genuine multipartite entanglement [S8]. If \mathcal{W} is an observable which has a positive expectation value on all biseparable states and a negative expectation value on the generated entangled state, we call this observable an entanglement witness. With the method introduced in Ref. [S9], the witness is constructed as

$$\mathcal{W} = \frac{1}{2} - |\psi\rangle\langle\psi| + |\psi'\rangle\langle\psi'|, \quad (\text{S.1})$$

where

$$|\psi'\rangle = \frac{1}{2} \left[|H\rangle^{\otimes 6} (|VV\rangle - |HH\rangle) + |V\rangle^{\otimes 6} (|HH\rangle + |VV\rangle) \right]$$

is an orthogonal state of $|\psi\rangle$, that is $\langle\psi|\psi'\rangle = 0$.

Then the witness is decomposed into a number of local von Neumann (or projective) measurements:

$$\begin{aligned} \mathcal{W} &= \frac{1}{2} - (|\psi\rangle\langle\psi| - |\psi'\rangle\langle\psi'|) \\ &= \frac{1}{2} - \frac{1}{2} \left[(|H\rangle\langle H|^{\otimes 6} - |V\rangle\langle V|^{\otimes 6})_{1-6} \otimes (|H\rangle\langle V|^{\otimes 2} + |V\rangle\langle H|^{\otimes 2})_{78} \right. \\ &\quad \left. + (|H\rangle\langle V|^{\otimes 6} + |V\rangle\langle H|^{\otimes 6})_{1-6} \otimes (|H\rangle\langle H|^{\otimes 2} - |V\rangle\langle V|^{\otimes 2})_{78} \right] \\ &= \frac{1}{2} - \left[\frac{1}{4} (|H\rangle\langle H|^{\otimes 6} - |V\rangle\langle V|^{\otimes 6})_{1-6} \otimes (X_7 X_8 - Y_7 Y_8) + \right. \\ &\quad \left. \frac{1}{12} \left(\sum_{k=0}^5 (-1)^k M_k^{\otimes 6} \right)_{1-6} \otimes (|H\rangle\langle H|^{\otimes 2} - |V\rangle\langle V|^{\otimes 2})_{78} \right], \end{aligned} \quad (\text{S.2})$$

where $M_k = [\cos(\frac{k\pi}{6})X + \sin(\frac{k\pi}{6})Y]$. The experimental results are shown in Fig. 4b in the main text, which yields

the witness $\langle W \rangle = -0.105 \pm 0.023$, which is negative by 4.5 standard deviations.

-
- [S1] Raussendorf, R., Harrington, J., Goyal, K. A fault-tolerant one-way quantum computer. *Ann. Phys.* **321**, 2242-2270 (2006).
- [S2] Dennis, E., Landahl, A., Kitaev, A. & Preskill, J. Topological quantum memory. *J. Math. Phys.* **43**, 44524505 (2002).
- [S3] Raussendorf, R., Harrington, J. Fault-tolerant quantum computation with high threshold in two dimensions. *Phys. Rev. Lett.* **98**, 190504 (2007).
- [S4] Raussendorf, R., Harrington, J., Goyal, K. Topological fault-tolerance in cluster state quantum computation. *New J. Phys.* **9**, 199 (2007).
- [S5] Raussendorf, R., Bravyi, S. & Harrington, J. Long-range quantum entanglement in noisy cluster states, *Phys. Rev. A* **71** 062313 (2005).
- [S6] Fowler, A. G., Goyal, K. Topological cluster state quantum computing. Preprint at <http://arxiv.org/abs/0805.3202> (2008).
- [S7] Fowler, A. G., Stephens, A. M., Groszkowski, P. High threshold universal quantum computation on the surface code. Preprint at <http://arxiv.org/abs/0803.0272> (2008).
- [S8] Bourennane, M., Eibl, M., Kurtsiefer, C., *et al.* Experimental detection of multipartite entanglement using witness operators. *Phys. Rev. Lett.* **92**, 087902 (2004).
- [S9] Gühne, O., Lu, C. Y., Gao, W. B., Pan, J. W. Toolbox for entanglement detection and fidelity estimation. *Phys. Rev. A* **76**, 030305 (2007).